

Photoluminescence from an emitter layer sandwiched between the stack of metasurfaces

Cite as: J. Appl. Phys. **129**, 183101 (2021); <https://doi.org/10.1063/5.0047352>

Submitted: 12 February 2021 . Accepted: 18 April 2021 . Published Online: 09 May 2021

 Shunsuke Murai, Kenichi Agata, and  Katsuhisa Tanaka

COLLECTIONS

Paper published as part of the special topic on [Emerging Materials and Devices for Efficient Light Generation](#)



View Online



Export Citation



CrossMark

ARTICLES YOU MAY BE INTERESTED IN

[Stick-and-play metasurfaces for directional light outcoupling](#)

Applied Physics Letters **118**, 021110 (2021); <https://doi.org/10.1063/5.0034115>

[Enhanced tunnel magnetoresistance in Mn-based perpendicular magnetic tunnel junctions utilizing antiferromagnetically coupled bcc-Co-based interlayer](#)

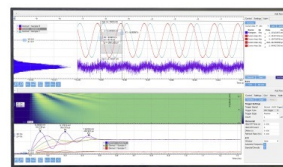
Applied Physics Letters **118**, 172412 (2021); <https://doi.org/10.1063/5.0042899>

[Large magnetic-field-induced strain at the magnetic order transition in triangular antiferromagnet AgCrS₂](#)

Applied Physics Letters **118**, 142404 (2021); <https://doi.org/10.1063/5.0046522>

Challenge us.

What are your needs for periodic signal detection?



Zurich
Instruments

Photoluminescence from an emitter layer sandwiched between the stack of metasurfaces

Cite as: J. Appl. Phys. **129**, 183101 (2021); doi: [10.1063/5.0047352](https://doi.org/10.1063/5.0047352)

Submitted: 12 February 2021 · Accepted: 18 April 2021 ·

Published Online: 10 May 2021



View Online



Export Citation



CrossMark

Shunsuke Murai,^{a)}  Kenichi Agata, and Katsuhisa Tanaka 

AFFILIATIONS

Department of Material Chemistry, Graduate School of Engineering, Kyoto University, Nishikyo-ku, Kyoto 615-8510, Japan

Note: This paper is part of the Special Topic on Emerging Materials and Devices for Efficient Light Generation

^{a)}Author to whom correspondence should be addressed: murai@dipole7.kuic.kyoto-u.ac.jp

ABSTRACT

The combination of metasurface with optical emitters provides a unique opportunity to control the emission. The metasurface effect strongly depends on the spectral overlap between the internal electronic transitions of the emitter and the optical resonances of the metasurface. Elaborate design of the metasurface could realize the resonances at both absorption and emission wavelengths of the emitter, but it usually leads to complexity in fabrication. In this work, we propose a very simple strategy to obtain the resonances at both wavelengths by sandwiching the emitter layer with a pair of metasurfaces designed for absorption and emission, respectively. For this purpose, we use a sticker of Al metasurface, which is the array of Al nanoparticles embedded in a flexible polymer film that can be stuck on any clean surfaces. The metasurface stack is prepared by simply placing the sticker, resonating at the emission wavelength, on the emitter layer deposited on the TiO₂ metasurface resonating at the absorption wavelength. The overall enhancement achieved for the stack of the metasurfaces can be understood roughly as the multiplication of contributions from the respective metasurfaces. Employing a sticker provides an easy-to-make way of constructing a stack of metasurfaces, which increases the degree of freedom in designing the metasurface-coupled emitters.

Published under an exclusive license by AIP Publishing. <https://doi.org/10.1063/5.0047352>

I. INTRODUCTION

Metallic and/or dielectric nanoparticles are regarded as optical nanoantenna that can receive/radiate light at the nanoscale.^{1–3} The effect of nanoantenna on the optical emitter is a well-studied topic in nano-optics.^{1,4–6} Nanoantenna can influence both on the absorption and emission wavelengths: For the absorption, the effect of antenna to increase the absorption of the emitter is known as pump enhancement.⁷ At the emission, two effects, quantum yield modification through modification of local density of optical state, known as the Purcell effect,^{8,9} and scattering of the emission out from the structure, known as outcoupling,⁵ could contribute to the overall emission properties. For nanoantennas with a broad resonance and/or for emitters with a small Stokes shift, both the absorption and emission wavelengths can be covered by a single nanoantenna.^{7,10} Using anisotropic nanoantennas, the simplest example of which is nanorods, is a sensible way of obtaining the double resonance.^{11,12} In such antennas, resonances along the short and long axes can be controlled independently, allowing for the modulation of both absorption and emission processes of the emitter. However, half

of the emitter is uncoupled to the resonance given the random orientation of the emitter.

The use of periodic arrays of nanoparticles, i.e., metasurfaces, increases the degree of freedom in designing the resonances, where the in-plane diffraction provides another channel of resonance in addition to the localized mode at each nanoparticle.^{13–20} In such arrays, detuning of the localized resonance with the diffraction allows for tuning the localized mode to the absorption and the lattice mode to the emission wavelength to cover both wavelengths by a single metasurface.²¹

While the single-metasurface approach to both the absorption and emission is simple and powerful, the separation of the role into two metasurfaces provides further flexibility in the spectral tuning of the emission. In this sense, the stack of metasurfaces, each separately designed for the absorption and emission wavelengths, should allow for the tuning of the emission properties with higher degree of freedom.²² However, the experiments so far focus on single-metasurface systems and the stacked metasurfaces have not been explored largely because of the complexity imposed on the sample preparation.^{23–28} The nanofabrication process requires the

flatness to the samples, and the presence of the first metasurface corrugates the surface and prohibits the fabrication of the second metasurface on the top.

We approach this problem from a different direction using the metasurface sticker which we developed recently.²⁹ The sticker consists of Al nanoparticle arrays embedded in a poly(dimethylsiloxane) (PDMS) film. The flexibility and adherence of PDMS to clean surfaces allow the sticker to be stuck on many surfaces without special treatments. Therefore, it brings about nanoantenna effects even on the materials that are incompatible with the fabrication process. We prepare the stack of metasurfaces by placing the sticker on another metasurface made of TiO₂ nanoparticle arrays with an emitter layer on the top. The photoluminescence from the sandwiched emitter is examined in comparison with the emitters coupled to the each metasurface separately.

II. SAMPLE DESIGN AND FABRICATION

The sample consists of the emitter layer sandwiched between the metasurfaces [see Fig. 1(a) for the sketch of the sample]. We employ as the emitter Lumogen F red 305 dye (BASF) dispersed in poly(methylmethacrylate) (PMMA). This dye shows the red emission upon excitation by blue light, with a high quantum yield and photo-stability. The first metasurface is designed for the pump enhancement. For this purpose, we selected the array of TiO₂ nanoparticles (diameter and height of 120 and 100 nm) arranged in the square lattice with the period of 260 nm [Fig. 1(b)]. TiO₂ was chosen because of the reasonably high refractive index and the transparency in the excitation wavelength of the emitter. In contrast, metallic nanoparticle has higher absorption in this region and may lower the absorption by the emitter. The TiO₂ metasurface was prepared via the oxidation of Ti nanoparticle arrays prepared by the lift-off process as described in a separate paper.³⁰ The emitter layer was deposited on the TiO₂ layer by a spin-coat with a thickness of ~600 nm.

Second metasurface for the emission wavelength is an Al metasurface sticker consisting of the Al nanoparticles (diameter and height of 220 and 200 nm) arranged in a hexagonal lattice with the period of 460 nm [Fig. 1(c)]. The Al metasurface was first made on the SiO₂ glass substrate coated by a sacrifice polymer layer, and then it was transferred to a PDMS film.²⁹ The second metasurface was stuck onto the emitter layer simply by placing it onto the surface.

III. RESULTS AND DISCUSSION

A. Angle-dependent extinction

Prior to the stack of metasurfaces, we measured the extinction of each metasurface separately. Extinction was defined as $1 - \text{direct (zeroth order) transmittance}$. The TiO₂ metasurface is transparent in the emission range of the emitter [see Fig. 2(a)]. The size of the TiO₂ nanoparticle is small compared to the wavelengths of the visible light, so the Mie resonance does not appear in the visible region. At shorter wavelengths, it shows the weak and sharp extinction features associated to the in-plane diffraction. The main extinction peak at $\lambda = 395$ nm and $\theta_{\text{in}} = 0^\circ$ splits and shifts as θ_{in} deviates from 0° , following the dotted lines representing the

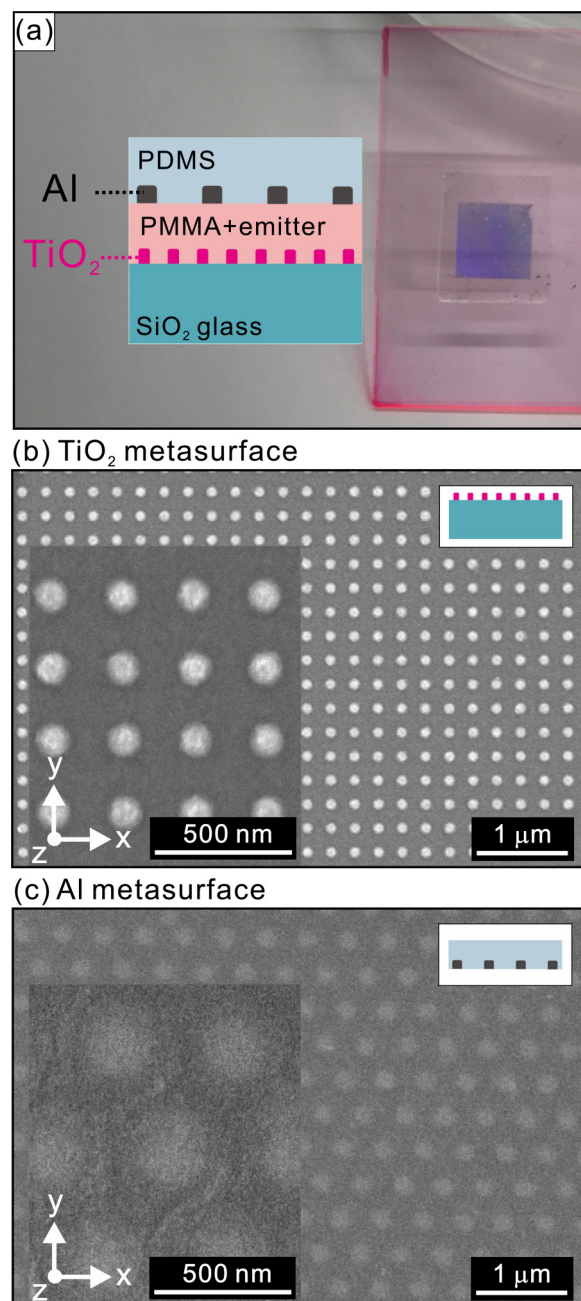


FIG. 1. (a) Cross-sectional sketch of the sandwiched system consisting of the stack of metasurfaces with an emitter layer in between. The top-view optical image of the sample is also shown. The SiO₂ glass substrate was 30×30 mm² in size, on which the TiO₂ metasurface (2×2 mm²) was fabricated. The emitter layer was spin-coated over the entire SiO₂ glass substrate, and the Al metasurface (6×6 mm²) embedded in PDMS was stuck onto the emitter layer. Top-view SEM images of (b) TiO₂ metasurface on the silica substrate and (c) Al metasurface embedded in PDMS. Insets are the cross-sectional sketch of the metasurface. The coordinates used in the optical measurements are also denoted.

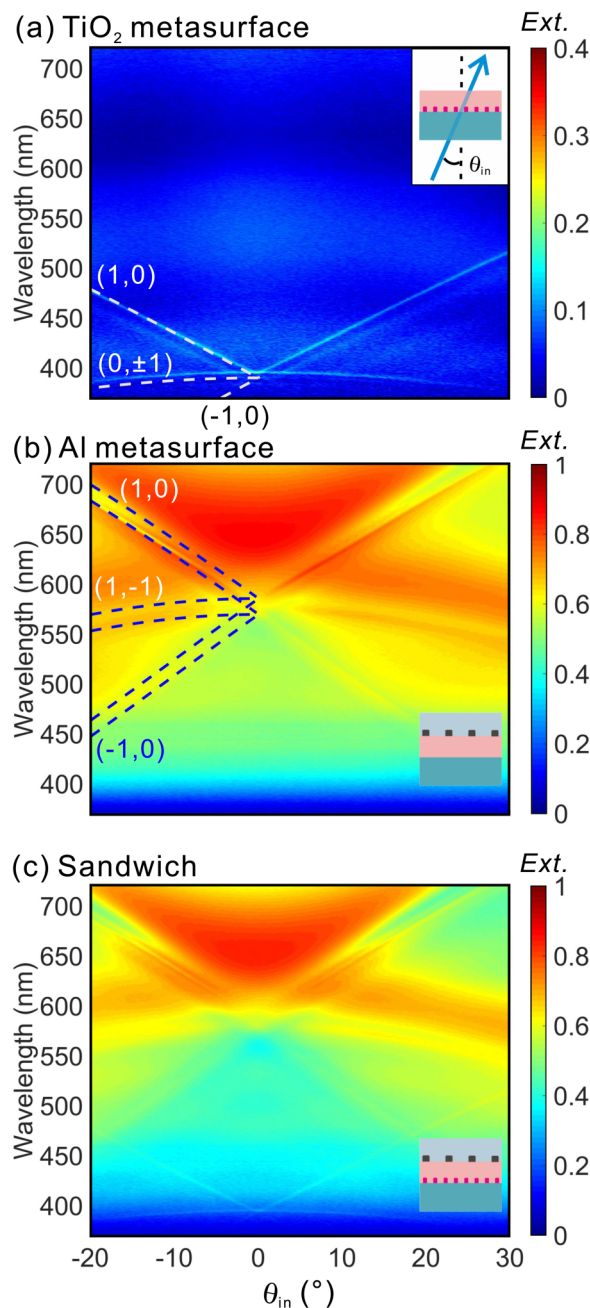


FIG. 2. Extinction spectra as a function of angle of incidence (θ_{in}) for the emitter layer with (a) the TiO_2 metasurface, (b) the Al metasurface and (c) for the sandwiched emitter layer between the Al and TiO_2 metasurfaces. θ_{in} is defined in the $z-x$ plane with the azimuthal angle from the x -direction being 0° (see the SEM images in Fig. 1 for the coordinate). Extinction is defined as 1 -direct transmittance [see the inset in (a) for the configuration]. The gray and blue dashed lines in (a) and (b), respectively, are the in-plane diffraction conditions for the square lattice with the period of 260 nm and for the hexagonal lattice with the period of 460 nm, respectively. Note that the color scale in (a) is different from the others.

dispersion of in-plane diffraction. The in-plane diffraction conditions or Rayleigh anomalies satisfy the following relation:

$$\vec{k}_0 = \vec{k}_{in}(\theta_{in}) \pm \vec{G}(m_1, m_2), \quad (1)$$

where \vec{k}_0 is the wave vector of the in-plane diffracted orders, \vec{k}_{in} is the in-plane component of the wave vector of the incident beam, and $\vec{G}(m_1, m_2) = m_1\vec{b}_1 + m_2\vec{b}_2$ is the reciprocal lattice vector of the array. For the square lattice, the unit vectors are $\vec{b}_1 = (2\pi/a)\vec{x}$, $\vec{b}_2 = (2\pi/a)\vec{y}$, with a the lattice constant ($a = 260$ nm), and m_1 and m_2 being the orders of diffraction.³¹ The gray dotted lines in the figure denote the diffraction conditions with $n = 1.5$ (PMMA) with the orders noted in the parentheses. The refractive index of PMMA is higher in this region compared to the visible region ($n = 1.47$). Because of the periodicity of 260 nm in a square lattice, the extinction of the TiO_2 metasurface appears only in the blue part of the visible.

The extinction of the Al metasurface sticker on the emitter layer [Fig. 2(b)] shows the lattice resonance in the visible because of the lattice design (hexagonal lattice with $a = 460$ nm). The reciprocal lattice vectors for the hexagonal array are $\vec{b}_1 = (\sqrt{2}\pi/a)(\vec{x} + \vec{y}/\sqrt{3})$ and $\vec{b}_2 = (\sqrt{2}\pi/a)(\vec{x} - \vec{y}/\sqrt{3})$. The $(1,0)$, $(1,-1)$, $(-1,0)$ diffraction orders are plotted using the refractive indices of PDMS ($n = 1.43$) and PMMA ($n = 1.47$). The in-plane diffraction is overlapping with the localized surface plasmon resonance of Al nanoparticles which is broad and extends over the visible region, and thus the extinction is much higher compared to that of the TiO_2 metasurface. The modification of the localized surface plasmon resonance along the diffraction means that both the plasmonic and diffraction modes are excited simultaneously as hybridized modes.³²

The extinction of the stacked metasurfaces [Fig. 2(c)] exhibits features of these two metasurfaces. No near-field interaction is expected between the two metasurfaces because the spectral position of the resonances, as well as their geometrical positions, are well separated. Only slight spectral shift is observed between the extinctions of the stacked and the separated metasurfaces. The shift in extinction will be discussed in comparison with the emission spectra in Sec. III B.

B. Angle-dependent emission

In order to optimize θ_{in} of the excitation beam for the pump enhancement, we measured the emission from the emitter layer with the TiO_2 metasurface upon irradiation with a $\lambda = 440.6$ nm laser at various θ_{in} . The beam was incident on the substrate side, and the emission from the other side was detected at a fixed angle of emission, $\theta_{em} = 10^\circ$ [see the inset of Fig. 3(a) for the configuration]. The enhancement factor, defined as the emission intensity from the sample divided by that from the reference emitter layer on the flat glass substrate, shows a maximum at $\theta_{in} = 11^\circ$ [Fig. 3(a)]. This angle corresponds to the angle where the $\lambda = 440.6$ nm light crosses the extinction feature due to in-plane diffraction [see Fig. 3(b) for the zoom-up extinction in the blue region]. At this condition, the excitation beam is scattered into the emitter layer which acts as a slab waveguide, where it is trapped and eventually absorbed by the dye molecules. We further confirm that this

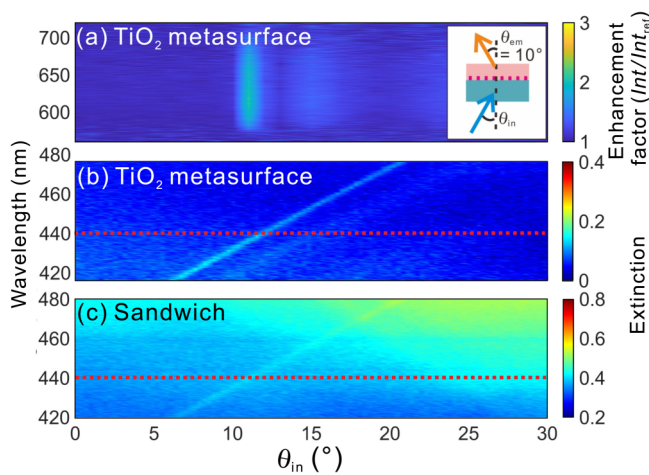


FIG. 3. Pump enhancement as a function of θ_{in} . (a) Photoluminescence enhancement (Int/Int_{ref}), defined as the emission intensity of the emitter layer on the metasurface normalized to that on the flat glass substrate, for the emitter layer with the TiO_2 metasurface. The sample was excited from the SiO_2 glass substrate side with the blue laser ($\lambda = 440.6$ nm) at various θ_{in} with a step of 1° and the emission from the other side was detected with a fixed emission angle, $\theta_{em} = 10^\circ$, defined in the $z-x$ plane. The inset is the sketch of the measurement configuration. (b) and (c) Extinction in the blue spectral region as a function of θ_{in} for the emitter layer with (b) the TiO_2 metasurface and (c) for the sandwiched emitter layer between the Al and TiO_2 metasurfaces. The data are the zoom-ups of those in Fig. 2. The dotted lines denote $\lambda = 440.6$ nm.

mode does not shift when the Al metasurface sticker is placed on the top [Fig. 3(c)].

Then, we measured the emission spectra with varied θ_{em} while θ_{in} being fixed at 11° . For the emitter layer on the TiO_2 metasurface, the enhancement is featureless as in Fig. 4(a). Because the lattice mode is in the blue region and the metasurface is transparent in the range of emission as in Fig. 2(a), no effect is expected on the emission process. In contrast, the diffraction mode in the blue indicates the pump enhancement. In parallel, for the emitter with the Al metasurface [Fig. 4(b)], the emission enhancement follows the diffraction line, showing the directional outcoupling; the emission trapped inside the emitter layer is scattered out into the direction defined by the lattice periodicity. When the emitter is sandwiched between the two metasurfaces [Fig. 4(c)], both pump enhancement and outcoupling occur: The angular profile is similar to the case of single Al metasurface, but the enhancement is higher because of the additional pump enhancement from the TiO_2 metasurface.

The spectral relation between the extinction and the emission is further examined by the cut of the spectra (Fig. 5). The extinction at $\theta_{in} = 10^\circ$ [Fig. 5(a)] for the TiO_2 metasurface is flat and small in the emission range of the emitter. The emission spectra at $\theta_{em} = 10^\circ$ [Fig. 5(b)] show that the enhancement factor achieved singly by the TiO_2 metasurface is around two irrespective of the emission wavelengths. Specifically at the peak wavelength of the emission from the reference layer on the flat substrate, $\lambda = 609$ nm, the value is 2.2. The extinction of the Al metasurface sticker at

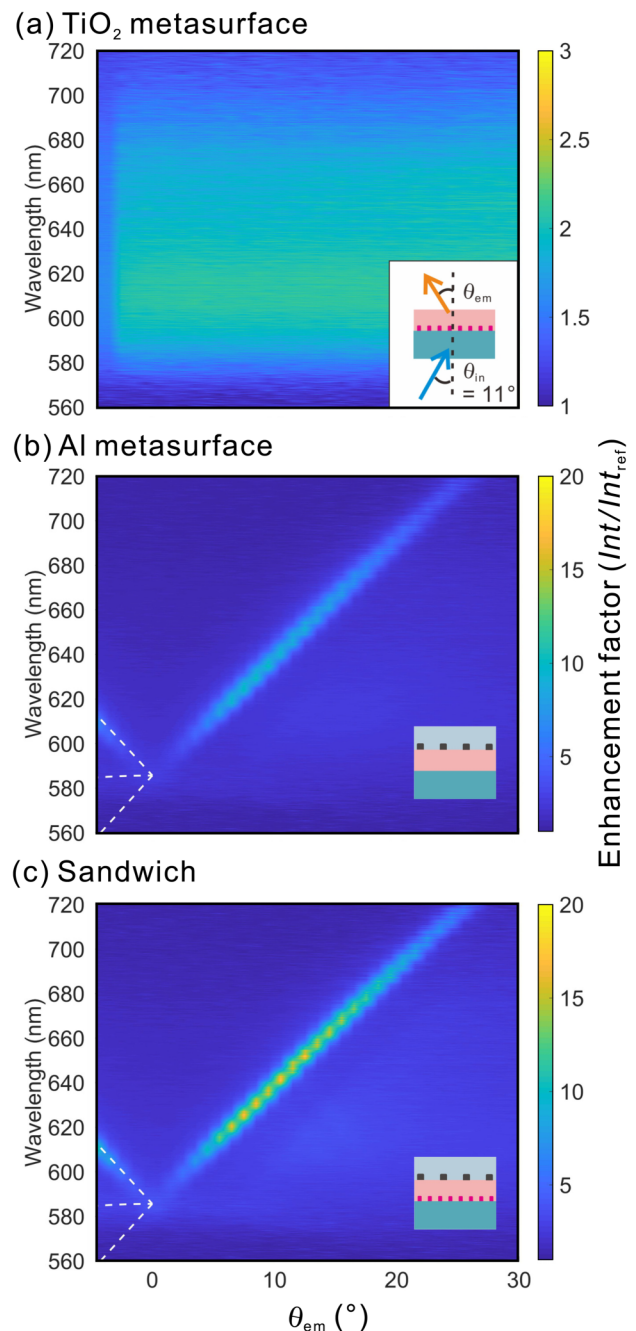


FIG. 4. Photoluminescence enhancement for the emitter layer (a) with the TiO_2 metasurface, (b) the Al metasurface, and (c) for the sandwiched emitter layer between the Al and TiO_2 metasurfaces. The samples were excited from the SiO_2 glass substrate side with the blue laser ($\lambda = 440.6$ nm) at $\theta_{in} = 11^\circ$. The emission from the other side was plotted as a function of emission angle, θ_{em} defined in the $z-x$ plane with the azimuthal angle from the x -direction being 0° . The white dashed lines in (b) and (c) denote the in-plane diffraction for the hexagonal lattice with the period of 460 nm and the refractive index of PMMA ($n = 1.47$). The insets show the sketch of the samples.

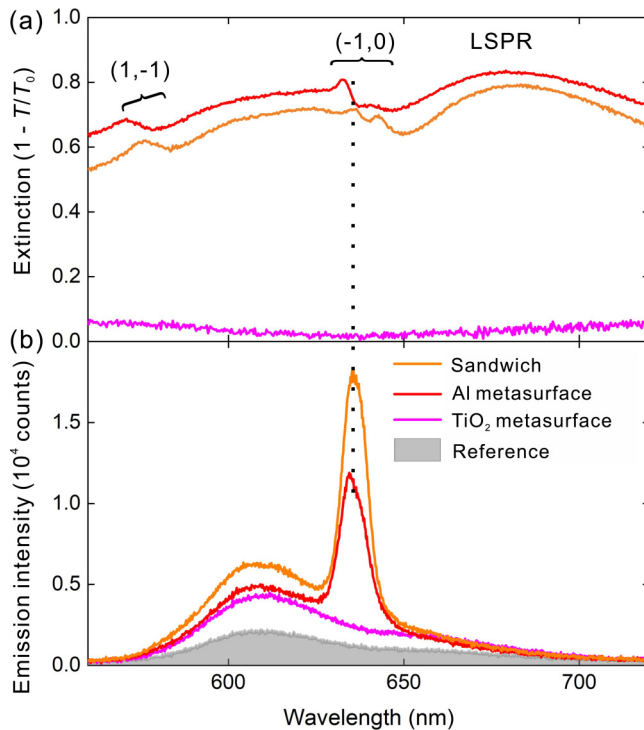


FIG. 5. (a) Extinction spectra at $\theta_{in} = 10^\circ$ for the emitter layer with the Al metasurface, the TiO_2 metasurface, and the layer sandwiched between the Al and TiO_2 metasurfaces. The spectral positions of the diffractions and localized surface plasmon resonance are also denoted. (b) Photoluminescence spectra at $\theta_{em} = 10^\circ$ for the reference emitter layer, and the emitter layer with the Al metasurface, the TiO_2 metasurface, and sandwiched between the Al and TiO_2 metasurfaces. The samples were excited from the backside with the blue laser ($\lambda = 440.6 \text{ nm}$) at $\theta_{in} = 11^\circ$. The vertical dotted line indicates the position of the emission peak of the sandwiched emitter.

$\theta_{in} = 10^\circ$ [Fig. 5(a)] shows several features corresponding to the diffraction orders, in addition to the broad peak at $\lambda \sim 690 \text{ nm}$ due to the localized surface plasmon resonance. The emission peak appearing at $\lambda = 634 \text{ nm}$ is associated to the $(-1,0)$ orders, verifying the outcoupling effect by the metasurface. The enhancement factor at the peak is around 9.8. It is noted that the emission enhancement occurs not only around the peak but also the entire spectral range. This flat enhancement overlapping the outcoupling indicates the presence of pump enhancement even for the single Al metasurface. The excitation beam hits the broad tail of the localized surface plasmon of the Al nanoparticles to increase the absorption by the emitters. The magnitude of the flat enhancement is also around two, and specifically 2.4 at $\lambda = 609 \text{ nm}$.

The addition of the Al metasurface to the TiO_2 metasurface slightly redshifts the extinction as seen in Fig. 5(a). Accordingly, the emission peak also redshifts to $\lambda = 636 \text{ nm}$ [Fig. 5(b)]. The pump enhancement is estimated to 3.1 times at $\lambda = 609 \text{ nm}$. This value is smaller compared to the pump enhancement from the TiO_2 metasurface multiplied by that of the Al metasurface

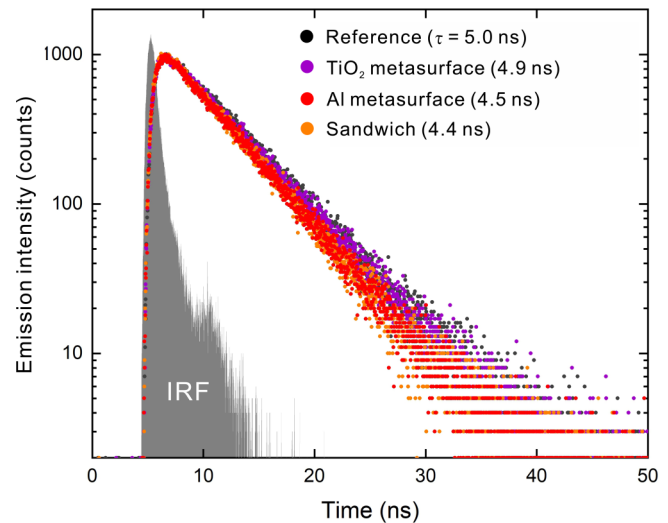


FIG. 6. (a) Emission lifetime measured for the reference emitter layer, and the emitter layer with the Al metasurface, the TiO_2 metasurface, and the layer sandwiched between the Al and TiO_2 metasurfaces. The instrumental response function (IRF) is also shown as a gray area. The samples were excited from the backside with the blue LED ($\lambda = 470 \text{ nm}$) and the emission intensity at $\lambda = 605 \text{ nm}$ was measured in a reflection configuration. The lifetimes extracted from the single-exponential fit to the decay are shown in the legend.

($2.2 \times 2.4 = 5.3$ at $\lambda = 609 \text{ nm}$). This 42% drop of enhancement indicates the interference of the pump enhancement when both the metasurfaces coexist. It is intuitively understood considering the situation where the sandwiched system is irradiated with the excitation beam; the excitation beam first hits the TiO_2 metasurface then the Al metasurface so that the spatial distribution of the scattering field is different from those of the single-metasurface systems.

While the pump enhancements from the stack of metasurfaces interfere, the pump enhancement and the outcoupling are independent and their combination will give the net enhancement which equals to the multiplication of the two effects. Indeed, the net enhancement for the sandwiched emitter, ~ 15.0 times at the peak wavelength of $\lambda = 636 \text{ nm}$, is similar to the multiplication of the enhancements for the TiO_2 and the Al metasurfaces ($2.0 \times 9.2 = 18.4$ at $\lambda = 636 \text{ nm}$). The smaller drop by 18% is ascribed to the fact that the single Al metasurface also gives the pump enhancement, which interferes with that of the TiO_2 metasurface.

C. Emission decay rate

The other factor contributing to the emission enhancement, i.e., the quantum yield modulation, was examined via emission decay rate (Fig. 6). Because the quantum yield is the ratio of radiative decay to the total decay rate, the change in quantum yield should be reflected on the change in temporal emission decay rate. The reference shows the single-exponential decay with the lifetime of $\tau = 5.0 \text{ ns}$. The PL lifetime slightly decreases for the emitter layer on the TiO_2 metasurface to 4.9 ns. The drop of the lifetime is

larger for the Al metasurface (4.5 ns) and the stack of metasurfaces (4.4 ns), which is expected given the high absorption of Al that provides an additional nonradiative decay channel for the emitter. It is noted that even for the largest drop for the stack of metasurfaces, the drop is only 10% of the reference, meaning that the change in quantum yield is small in the present system. This is because the thickness of the emitter layer is 600 nm and only the emitters in the vicinity of the metasurface are affected by the antenna.³³ For the good emitter with high quantum yield as the present dye, the additional decay channel created by the antenna in many cases decreases the emission intensity.³⁴ Therefore, the limited modulation of quantum yield for a thick emitter layer is beneficial for the emission enhancement. More than 10 times emission enhancement due to the pump enhancement and outcoupling without the Purcell effect has been reported by combining thick and high-quantum-yield emitter layers with metasurfaces.^{16,21,31}

IV. CONCLUSION

In summary, we evaluated the emission modulation by the stack of metasurfaces designed separately to modulate the incoupling of excitation beam and outcoupling of the emission. The stack of metasurfaces was prepared by simply placing the sticker of Al metasurface on top of the emitter layer on another metasurface consisting of TiO₂ nanoparticles. The total emission enhancement is understood by the multiplication of the separate contributions from the two metasurfaces. The results show that the pump enhancement and the outcoupling are independent at separated wavelengths and do not interfere each other, which makes the design of the stack of metasurfaces simple and straightforward. It is noted that the design of the stacked system including the size of nanoparticles and the thickness of the emitter layer is not fully optimized, and there is room for improvement for the enhancement. This proof-of-concept work using the downconversion emitter can be easily extended to the frequency-conversion systems such as upconversion³⁵ and second harmonic generation.

V. METHOD

A. Fabrication of Al metasurface sticker

Al nanoparticle arrays embedded in PDMS were fabricated following the method described in Ref. 29. In short, Al thin film (thickness = 200 nm) was grown on the SiO₂ glass substrate covered by a polyvinylpyrrolidone (PVP) layer (500 nm thick), which serves as a sacrifice layer. Then, the Al nanoparticle array was fabricated by using nanoimprint lithography (EntreTM3, Obducat) and reactive ion etching (RIE) (RIE-101iPH, Samco). Then, ingredients of PDMS (DOWSILTM SILPOT 184 Dow) were mixed and cast onto the Al nanoparticle array on the substrate (thickness ~ 2 mm), degassed under vacuum for 40 min at 35 °C and then cured for 2 h at 80 °C. The array with a PDMS film on the top was soaked in distilled water for one day to dissolve the sacrifice PVP layer. Finally, the PDMS film embedded with the Al nanoparticle array was peeled off from the glass substrate. The size of the Al nanoparticle and the period of the array were confirmed by scanning electron microscopy (SEM, SU8000, Hitachi).

B. Fabrication of TiO₂ metasurface

TiO₂ metasurface was fabricated via oxidation of Ti metasurface as described in Ref. 30. First, the resist (ZEP520A) was coated onto an SiO₂ glass substrate and the resist was nanopatterned by electron-beam lithography (F7000s-KYT01, Advantest) followed by developing with a developer (ZED-N50). Then, the Ti thin film (thickness = 100 nm) was grown on the prepatterned resist on the substrate using electron beam deposition. Finally, a lift-off process was performed with a solvent (Microremover 1165) to remove the excess Ti on the resist. Finally, the Ti metasurface was converted into TiO₂ by the heat treatment in an electric furnace for 5 min in air. The size of the TiO₂ nanoparticle and the period of the array were confirmed by SEM. As an emitter layer, a PMMA layer containing 3 wt% Lumogen F red 305 (~600 nm) was prepared by spin-coating.

C. Transmittance measurements

Angular-varied extinction spectra were measured as a function of angle of incidence θ_{in} collected by a fiber (numerical aperture = 0.22) coupled to the spectrometer (Flame-S, Ocean Optics). The sample was set on a rotation stage to vary θ_{in} on the sample surface with a step of 0.3°. The light source was an unpolarized halogen lamp (SLS201L/M, Tholab), with the emitter layer without the metasurface on the SiO₂ glass substrate as a reference. Extinction was defined as $E = 1 - T/T_0$, with T and T_0 being the measured zeroth-order transmission of the sample and the reference, respectively.

D. Emission measurements

A diode-pumped solid-state laser ($\lambda = 440.6$ nm, Laser Century BLS445, incident laser power = 10 mW) was incident on the SiO₂ glass substrate side at $\theta_{in} = 11^\circ$ from the normal. An optical fiber coupled to the spectrometer was rotated around the sample to obtain the emission spectrum through the metasurface as a function of emission angle θ_{em} with a step of 1°. The emission decay at the main luminescence peak ($\lambda = 605$ nm) was measured using a time-correlated single-photon counting module (Quantaaurus-Tau, Hamamatsu Photonics) equipped with a pulsed LED ($\lambda = 470$ nm, temporal resolution of 0.7 ns) as an excitation source. The decay curve was fitted to the single exponential function after deconvolution using the instrumental response function (IRF).

ACKNOWLEDGMENTS

This work was partly supported by the Nanotechnology Hub, Kyoto University (No. JPMXP09F19NMC042). We gratefully acknowledge financial support from Kakenhi (Nos. 19K22055, 19K22058, and 19H02434), MEXT, Japan and the Masuya Memorial Basic Research Foundation.

DATA AVAILABILITY

The data that support the findings of this study are available from the corresponding author upon reasonable request.

REFERENCES

- ¹P. Anger, P. Bharadwaj, and L. Novotny, "Enhancement and quenching of single-molecule fluorescence," *Phys. Rev. Lett.* **96**, 113002 (2006).
- ²V. Giannini, A. I. Fernández-Domínguez, S. C. Heck, and S. A. Maier, "Plasmonic nanoantennas: Fundamentals and their use in controlling the radiative properties of nanoemitters," *Chem. Rev.* **111**, 3888–3912 (2011).
- ³T. Coenen, E. J. R. Vesseur, A. Polman, and A. F. Koenderink, "Directional emission from plasmonic Yagi-Uda antennas probed by angle-resolved cathodoluminescence spectroscopy," *Nano Lett.* **11**, 3779–3784 (2011).
- ⁴P. Bharadwaj, B. Deutsch, and L. Novotny, "Optical antennas," *Adv. Opt. Photonics* **1**, 438 (2009).
- ⁵G. Lozano, S. R. K. Rodriguez, M. A. Verschuuren, and J. Gómez Rivas, "Metallic nanostructures for efficient LED lighting," *Light Sci. Appl.* **5**, e16080 (2016).
- ⁶T. Kosako, Y. Kadoya, and H. F. Hofmann, "Directional control of light by a nano-optical Yagi-Uda antenna," *Nat. Photonics* **4**, 312–315 (2010).
- ⁷A. Kinkhabwala, Z. Yu, S. Fan, Y. Avlasevich, K. Müllen, and W. E. Moerner, "Large single-molecule fluorescence enhancements produced by a bowtie nanoantenna," *Nat. Photonics* **3**, 654 (2009).
- ⁸W. L. Barnes, "Fluorescence near interfaces: The role of photonic mode density," *J. Mod. Opt.* **45**, 661–699 (1998).
- ⁹K. Okamoto, I. Niki, A. Shvartser, Y. Narukawa, T. Mukai, and A. Scherer, "Surface-plasmon-enhanced light emitters based on InGaN quantum wells," *Nat. Mater.* **3**, 601 (2004).
- ¹⁰K. Tawa, M. Umetsu, H. Nakazawa, T. Hattori, and I. Kumagai, "Application of 300 enhanced fluorescence on a plasmonic chip modified with a bispecific antibody to a sensitive immunosensor," *ACS Appl. Mater. Interfaces* **5**, 8628–8632 (2013).
- ¹¹S.-Y. Liu, L. Huang, J.-F. Li, C. Wang, Q. Li, H.-X. Xu, H.-L. Guo, Z.-M. Meng, Z. Shi, and Z.-Y. Li, "Simultaneous excitation and emission enhancement of fluorescence assisted by double plasmon modes of gold nanorods," *J. Phys. Chem. C* **117**, 10636–10642 (2013).
- ¹²H. Wang, B. Zhang, Y. Zhao, X. Chen, Z. Zhang, and H. Song, "Integrated effects of near-field enhancement-induced excitation and surface plasmon-coupled emission of elongated gold nanocrystals on fluorescence enhancement and the applications in LEDs," *ACS Appl. Electron. Mater.* **1**, 2116–2123 (2019).
- ¹³S. Zou, N. Janel, and G. C. Schatz, "Silver nanoparticle array structures that produce remarkably narrow plasmon lineshapes," *J. Chem. Phys.* **120**, 10871 (2004).
- ¹⁴B. Auguié and W. L. Barnes, "Collective resonances in gold nanoparticle arrays," *Phys. Rev. Lett.* **101**, 143902 (2008).
- ¹⁵Y. Z. Chu, E. Schonbrun, T. Yang, and K. B. Crozier, "Experimental observation of narrow surface plasmon resonances in gold nanoparticle arrays," *Appl. Phys. Lett.* **93**, 181108 (2008).
- ¹⁶S. Murai, M. A. Verschuuren, G. Lozano, G. Pirruccio, S. R. K. Rodriguez, and J. G. Rivas, "Hybrid plasmonic-photonic modes in diffractive arrays of nanoparticles coupled to light-emitting optical waveguides," *Opt. Express* **21**, 4250–4262 (2013).
- ¹⁷W. Wang, M. Ramezani, A. I. Väkeväinen, P. Törmä, J. G. Rivas, and T. W. Odom, "The rich photonic world of plasmonic nanoparticle arrays," *Mater. Today* **21**, 303–314 (2018).
- ¹⁸V. G. Kravets, A. V. Kabashin, W. L. Barnes, and A. N. Grigorenko, "Plasmonic surface lattice resonances: A review of properties and applications," *Chem. Rev.* **118**, 5912–5951 (2018).
- ¹⁹I. M. Hancu, A. G. Curto, M. Castro-López, M. Kuttge, and N. F. van Hulst, "Multipolar interference for directed light emission," *Nano Lett.* **14**, 166–171 (2014).
- ²⁰D. Khlopin, F. Laux, W. P. Wardley, J. Martin, G. A. Wurtz, J. Plain, A. V. Zayats, W. Dickson, and D. Gerard, "Lattice modes and plasmonic linewidth engineering in gold and aluminum nanoparticle arrays," *J. Opt. Soc. Am. B* **34**, 691 (2017).
- ²¹G. Lozano, D. J. Louwers, S. R. K. Rodriguez, S. Murai, O. T. A. Jansen, M. A. Verschuuren, and J. G. Rivas, "Plasmonics for solid-state lighting: Enhanced excitation and directional emission of highly efficient light sources," *Light Sci. Appl.* **2**, e66 (2013).
- ²²I. M. Fradkin, S. A. Dyakov, and N. A. Gippius, "Thickness-independent narrow resonance in a stack of plasmonic lattices," *Phys. Rev. Appl.* **14**, 054030 (2020).
- ²³D. Dregely, R. Taubert, J. Dorfmüller, R. Vogelgesang, K. Kern, and H. Giessen, "3D optical Yagi-Uda nanoantenna array," *Nat. Commun.* **2**, 267 (2011).
- ²⁴K. Tanaka, D. Arslan, S. Fasold, M. Steinert, J. Sautter, M. Falkner, T. Pertsch, M. Decker, and I. Staude, "Chiral bilayer all-dielectric metasurfaces," *ACS Nano* **14**, 15926–15935 (2020).
- ²⁵Z. Wu, X. Chen, M. Wang, J. Dong, and Y. Zheng, "High-performance ultrathin active chiral metamaterials," *ACS Nano* **12**, 5030–5041 (2018).
- ²⁶N. Liu, H. Guo, L. Fu, S. Kaiser, H. Schweizer, and H. Giessen, "Three-dimensional photonic metamaterials at optical frequencies," *Nat. Mater.* **7**, 31–37 (2008).
- ²⁷G. Subramania and S. Y. Lin, "Fabrication of three-dimensional photonic crystal with alignment based on electron beam lithography," *Appl. Phys. Lett.* **85**, 5037–5039 (2004).
- ²⁸A. S. P. Chang, Y. S. Kim, M. Chen, Z.-P. Yang, J. A. Bur, S.-Y. Lin, and K.-M. Ho, "Visible three-dimensional metallic photonic crystal with non-localized propagating modes beyond waveguide cutoff," *Opt. Express* **15**, 8428–8437 (2007).
- ²⁹K. Agata, S. Murai, and K. Tanaka, "Stick-and-play metasurfaces for directional light outcoupling," *Appl. Phys. Lett.* **118**, 021110 (2021).
- ³⁰S. Murai, F. Zhang, K. Aichi, and K. Tanaka, "Oxidation pathway to the TiO₂ metasurface for harnessing photoluminescence," *J. Appl. Phys.* **129**, 163101 (2021).
- ³¹S. Murai, M. Saito, H. Sakamoto, M. Yamamoto, R. Kamakura, T. Nakanishi, K. Fujita, M. Verschuuren, Y. Hasegawa, and K. Tanaka, "Directional outcoupling of photoluminescence from Eu (III)-complex thin films by plasmonic array," *APL Photonics* **2**, 026104 (2017).
- ³²G. Vecchi, V. Giannini, and J. Gómez Rivas, "Surface modes in plasmonic crystals induced by diffractive coupling of nanoantennas," *Phys. Rev. B: Condens. Matter Mater. Phys.* **80**, 201401 (2009).
- ³³Y. Kawachiya, S. Murai, M. Saito, K. Fujita, and K. Tanaka, "Photoluminescence decay rate of an emitter layer on an aluminum cylinder array: Effect of layer thickness," *J. Opt. Soc. Am. B* **36**, E1–E8 (2019).
- ³⁴R. Kamakura, S. Murai, Y. Yokobayashi, K. Takashima, M. Kuramoto, K. Fujita, and K. Tanaka, "Enhanced photoluminescence and directional white-light generation by plasmonic array," *J. Appl. Phys.* **124**, 213105 (2018).
- ³⁵Y. Gao, S. Murai, K. Shinozaki, S. Ishii, and K. Tanaka, "Aluminum for near infrared plasmonics: Amplified up-conversion photoluminescence from core-shell nanoparticles on periodic lattices," *Adv. Opt. Mater.* **9**, 2001040 (2021).